Deep learning-based polarization feature retrieval from a single Stokes vector

Conference Paper · March 2022

DOI: 10.1117/12.2609583

5 authors, including:

Tongyu Huang
Tsinghua University
21 PUBLICATIONS **148** CITATIONS
SEE PROFILE

Hui Ma
Tsinghua University
411 PUBLICATIONS **6,740** CITATIONS
SEE PROFILE

Deep learning-based polarization feature retrieval from a single Stokes vector

Lu Si, Tongyu Huang, Xingjian Wang, Yue Yao, Hui Ma

Lu Si, Tongyu Huang, Xingjian Wang, Yue Yao, Hui Ma, "Deep learning-based polarization feature retrieval from a single Stokes vector," Proc. SPIE 11963, Polarized Light and Optical Angular Momentum for Biomedical Diagnostics 2022, 1196307 (4 March 2022); doi: 10.1117/12.2609583

SPIE.

Event: SPIE BiOS, 2022, San Francisco, California, United States

Deep Learning-based Polarization Feature Retrieval from A Single Stokes Vector

Lu Si[a], Tongyu Huang[bc], Xingjian Wang[a], Yue Yao[a], and Hui Ma[abcd]

[a]Tsinghua-Berkeley Shenzhen Institute, Tsinghua University, Shenzhen 518071, China
[b]Shenzhen International Graduate School, Tsinghua University, Shenzhen 518055, China
[c]Department of Biomedical Engineering, Tsinghua University, Beijing 100084, China
[d]Department of Physics, Tsinghua University, Beijing 100084, China

ABSTRACT

Polarization is capable of probing microstructures and has unique sensitivity to fibrous anisotropic structure. Polarimetric imaging has demonstrated promising potential in diverse applications ranging from biomedicine, material science, and atmospheric remote sensing. The polarization properties of samples can be comprehensively described by a Mueller matrix (MM). However, the relationship between individual MM elements and properties of the sample is often not clear. There have been consistent efforts to derive polarization parameters from MM based on certain assumptions for better description of the samples, e.g., MM polar decomposition (MMPD), MM transformation (MMT) and MM differential decomposition. Usually, the MM imaging requires sequential measurements with different polarization states of incident light and the imaging process is time consuming. In addition, for movable samples, we cannot guarantee the consistency during the imaging. This may cause precision issues since the images cannot be well-registered. In this work, we built a statistical translation model to generate polarization parameters from a single Stokes vector which can be obtained by one-shot imaging. This will improve the imaging efficiency, simplify the optical system and avoid introducing errors by the image registration. In the model design, we adopted the generative adversarial network (GAN) where the generator is based on a U-net architecture. We demonstrated the effectiveness of our approach on liver tissue, blood smear and porous anodic alumina (PAA) film, and quantitatively evaluated the results by similarity assessment methods. The model can generate a parameter image within 0.1 second on a desktop computer, which shows the potential to achieve real-time performance.

Keywords: Polarimetric imaging, Deep learning, Mueller matrix, Stokes vector

1. INTRODUCTION

Mueller matrix (MM) is a comprehensive representation of the polarization transformation properties of turbid media. It can provide rich information about the microstructure of biomedical samples.[1] However, the acquisition of a MM requires multiple exposures, which makes the quality of measurements very sensitive to small changes in the light source, and sample and optical alignments among different exposures.

The experimental setup of MM polarimetry can be designed by adding the polarization states generator (PSG) and analyzer (PSA) to the non-polarization optical path.[2] Traditionally, to resolve the 16 elements of the MM, at least 16 independent intensity images must be measured under different polarization modulations.[3] Considering the precision and efficacy, there are various MM polarimetry methods have been proposed. For example, by rotating both the polarizers and retarders in PSG and PSA, all six polarization components (linear 0°, 45°, 90°, 135°, right- and left-hand circular polarization states) corresponding to each incident and emerging light state can be measured one by one. Another widely used MM polarimetry is the dual-rotating retarder method where the polarizers are fixed in both PSG and PSA, and two retarders are rotated with a fixed ratio of angles.[4–6] Multi-exposure is time consuming while MM polarimetry can be easily affected to movement or polarization property changes during the measurement. For rapidly changing or dynamic objects, it might be some limitations for time-sequenced MM polarimeters above. To reduce the number of exposures, Chang et al.[7]

Hui Ma: E-mail: mahui@tsinghua.edu.cn

Polarized Light and Optical Angular Momentum for Biomedical Diagnostics 2022, edited by Jessica C. Ramella-Roman, Hui Ma, Tatiana Novikova, Daniel S. Elson, I. Alex Vitkin, Proc. of SPIE Vol. 11963, 1196307 ·
 · 1605-7422 · doi: 10.1117/12.2609583

and Huang et al.[8] used the division of the focal plane (DoFP) polarimeters in the microscope, which can capture the Stokes vector images in a single shot. The full MM can be resolved through four times of exposure in this method.[8] Furthermore, the concepts of snapshot MM polarimeters have been proposed. Piquero et al. used the full Poincare beams and wavefront division to resolve the MM.[9] Dubreuil et al.[10] and Hagen et al.[11] used wavelength-dependent birefringent media to take different measurements in parallel. However, these snapshot techniques can only be used on homogeneous medium, and not suitable to the imaging of complex samples, e.g., tissue slices. This limits their usage in practice.

In this work, we take the advantage of DoFP to obtain the Stokes images in a single shot, and then feed Stokes images to a well-designed deep learning network to generate MM-based polarization parameter images (as shown in Figure 1). The Stokes polarimetry is simply configured, and there are no moving or active parts in the imaging system when the pre-trained model is built. This will reduce the probability of unexpected errors from mechanical movements.

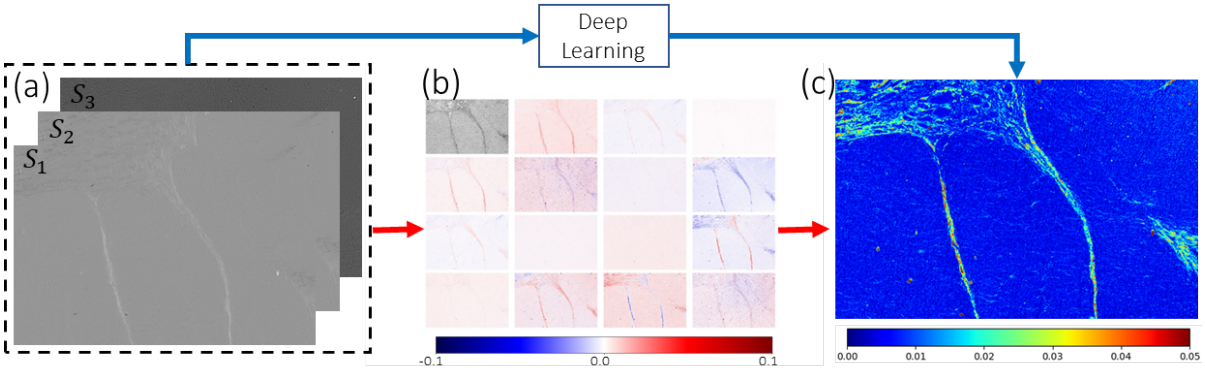

Figure 1. Traditional (red arrow) and deep learning-based (blue arrow) workflows of MM-derived parameter generation. (a) Stokes image of S_1, S_2 and S_3 channels. (b) Experimental MM element images. (c) The MMPD-δ image of a liver fibrosis tissue sample.

2. STOKES AND MUELLER MATRIX POLARIMETRY

Deep learning models usually require huge amounts of data in the training stage. In the data collection procedure, we used the MM microscope based on dual division of focal plane polarimeters (DoFPs-MMM).[8] As shown in Figure. 2 (a) and (b), in DoFPs-MMM, the PSA is capable of detecting the full polarization states simultaneously by adopting two DoFP polarimeters (DoFP CCD: PHX050S-PC, Lucid Vision Labs, Canada), one of which is equipped with a fixed quarter-wave plate R2 (Daheng Optics, China). The PSG consists of a fixed-angle polarizer P1 (Daheng Optics, China) and a rotatable quarter-wave plate R1 (Daheng Optics, China). The light emitted from the LED (3W, 632 nm, $\Delta\lambda = 20$ nm), undergoes the polarization modulation by the PSG, passes through the sample and analyzed by the PSA. The PSA is calibrated by a standard polarization light source or a PSG, and four independent polarization states will be detected and analyzed to reconstruct 8×4 instrument matrix of PSA. The instrument matrix is calculated pixel by pixel. To calculate MM of the sample, the quarter-wave plate R1 in the PSG rotates to four preset angles to generate 4 independent incident polarization states, as shown in Figure 2 (c), which compose the instrument matrix $[\boldsymbol{S}_{\text{in}}]$ of the PSG. After the light interacted with sample, 4 corresponding Stokes vectors $[\boldsymbol{S}_{\text{out}}]$ of outgoing light are measured by the PSA consisting of dual DoFP polarimeters. Finally, the MM of the sample can be reconstructed according to $\boldsymbol{M} = [\boldsymbol{S}_{\text{out}}]\,[\boldsymbol{S}_{\text{in}}]^{-1}$.[8]

The polarization properties of samples can be comprehensively described by a MM. However, the relationship between individual MM elements and properties of the sample is often not clear. MM polar decomposition (MMPD)[12] describes tissue-like media appropriately, and has been validated in many biomedical applications.[1,2] MMPD assumes the optical effects is serial following the order as diattenuation ($\boldsymbol{M}_D$), retardation ($\boldsymbol{M}_R$) and general depolarization ($\boldsymbol{M}_\Delta$), and is decomposed in a product form as $\boldsymbol{M} = \boldsymbol{M}_\Delta \boldsymbol{M}_R \boldsymbol{M}_D$. In this work, we train the deep learning model to translate Stokes images to MMPD parameter images directly. Especially, we focus

on the linear retardance parameter $\delta = \arccos\left(\sqrt{\left(M_{R22}+M_{R33}\right)^2+\left(M_{R32}-M_{R23}\right)^2}-1\right)$ and diattenuation parameter $D=\sqrt{M_{12}^2+M_{13}^2+M_{14}^2}$. Before feeding into the model, the Stokes image of S_1, S_2 and S_3 channels are normalized by the S_0 component pixel by pixel.

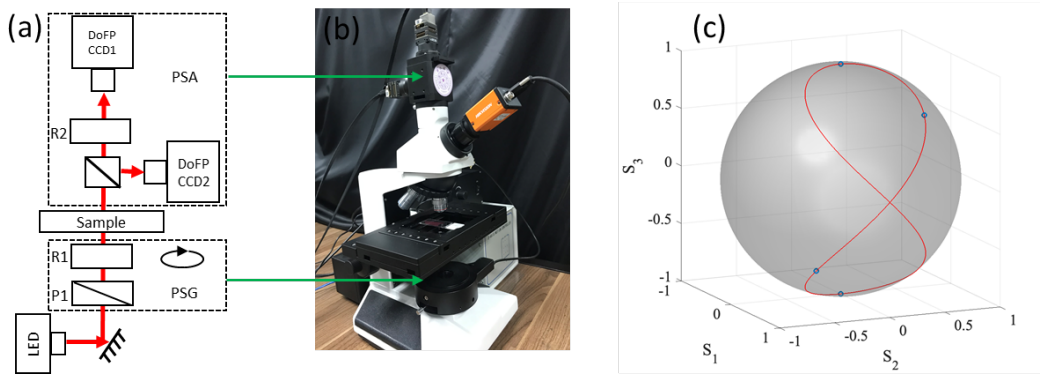

Figure 2. The experimental setup. (a) Diagram of DoFPs MM microscope. (b) Photograph of DoFPs-MM microscope. (c) Incident polarization states on Poincare sphere.

3. GENERATIVE ADVERSARIAL NETWORKS

We use conditional generative adversarial networks (GAN)[13] to generate MM-derived parameter images from Stokes images. We define the data domains of Stokes vector and MM-derived parameter as X and Y respectively, and define the generator network as G and the discriminator as D. In the training phase, Stokes image $x \in X$ is fed into the generator model to generate realistic parameter images, while the discriminator model tries to classify whether the parameter image is real or synthetic. These two models are trained together in a zero-sum game adversarially, until the whole architecture converges. The flowchart of the architecture is illustrated in Figure 3. Besides the GAN loss function, in this image-to-image translation, we use L1 and structural similarity index (SSIM)[14] losses to measure the similarity between generated and real images in the pixel and image levels respective. Furthermore, to reduce noise, total variance (TV) loss is introduced to improve the image quality of generated parameters. In this work, we use a U-net-based encoder-decoder network[15] as the generator and a PatchGAN discriminator.[16] The details of the neural networks are discussed in our previous work.[17] In both training and testing stage, the patch size is fixed as 256×256.

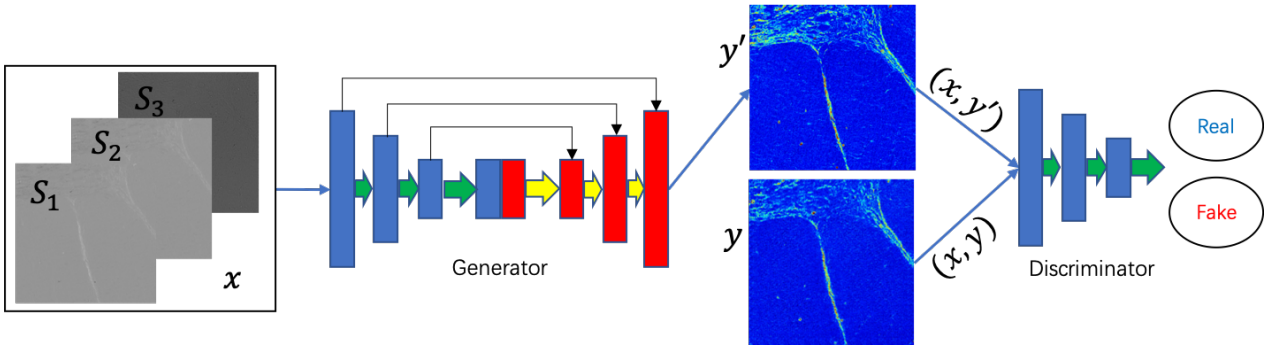

Figure 3. Flowchart of conditional generative adversarial network in the training and testing stages.

4. EXPERIMENTAL RESULTS

We conducted the experiments on three types of samples, i.e., sectioned liver tissues, blood smears and porous anodic alumina (PAA). The liver samples were prepared by the Mengchao Hepatobiliary Hospital of Fujian

Medical University. The blood smear samples were prepared by University of Chinese Academy of Science Shenzhen Hospital. All works were approved by the Ethics Committee of these two hospitals. PAA is a photonic crystal with a porous structure with obvious optical anisotropy caused by birefringence, which is widely used to fabricate the nanostructure arrays or microfilters. Our previous works show that the optical axis orientation of regions is related to various factors in the production process.[18] We deployed the model on a desktop computer with Intel Core-i9-9900K and a Geforce GTX 2080Ti card. When the model is well built in the training, the prediction time of one patch is less than 0.1 second.

Figure 4 illustrates the generated results of three samples. For liver fibrosis tissue and PAA, we predicted the linear retardance parameter MMPD-δ, while we focused on the diattenuation parameter of blood smear. We used normalized root mean square error (NRMSE) and peak signal-to-noise (PSNR) to quantitatively evaluate the performance of our model. NRMSE and PSNR measure the similarity between the generated and ground truth images in the pixel and image level respectively. As we can see, the structures of the output are clear and the pixel values are close to the ground truth.

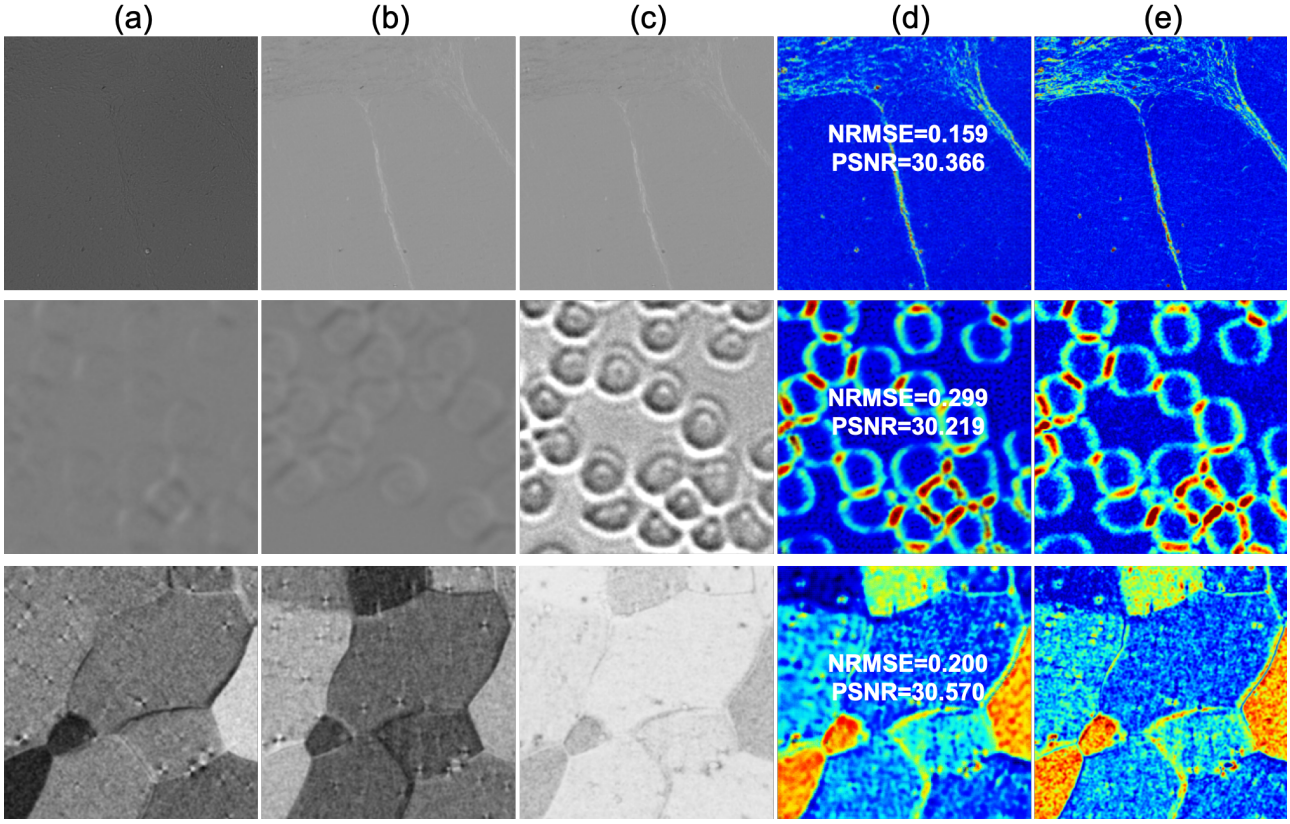

Figure 4. Experimental results of liver tissue MMPD-δ image (first row), blood smear MMPD-D image (second row) and PAA MMPD-δ image (third row). (a), (b) and (c) are normalized Stokes images of S_1, S_2 and S_3 channels illuminated by right-hand circular polarized light. (d) Generated parameter images based on the deep learning model. (e) Corresponding ground truth parameter images.

5. CONCLUSIONS

In this work, we propose a deep learning-based method to generate Mueller matrix polar decomposition parameter images from a single Stokes image. We adopted the conditional generative adversarial network to learn the statistical translation from Stokes to parameter images. We demonstrated the efficacy of our approach on liver tissues, blood smears and porous anodic alumina samples. This method will effectively suppress errors due

to system instability and sample variation during the data acquisition process, and reduces the challenges in hardware design.

ACKNOWLEDGMENTS

This work has been supported by National Key Research and Development Program of China (2018YFC1406600), National Natural Science Foundation of China (NSFC) (No. 11974206 and No.61527826) and Guangdong Development Project of Science and Technology (2020B1111040001). We thank Mengchao Hepatobiliary Hospital of Fujian Medical University and University of Chinese Academy of Sciences Shenzhen Hospital for the sample preparation. We thank Ruiqi Huang and Zhi Wang for helpful discussions.

REFERENCES

[1] He, C., He, H., Chang, J., Chen, B., Ma, H., and Booth, M. J., "Polarisation optics for biomedical and clinical applications: a review," *Light, Science & Applications* **10**, 1–20 (2021).

[2] He, H., Liao, R., Zeng, N., Li, P., Chen, Z., Liu, X., and Ma, H., "Mueller matrix polarimetry—an emerging new tool for characterizing the microstructural feature of complex biological specimen," *Journal of Lightwave Technology* **37**, 2534–2548 (2019).

[3] Le Gratiet, A., Mohebi, A., Callegari, F., Bianchini, P., and Diaspro, A., "Review on complete mueller matrix optical scanning microscopy imaging," *Applied Sciences* **11**(4), 1632 (2021).

[4] Azzam, R. M. A., "Photopolarimetric measurement of the Mueller matrix by fourier analysis of a single detected signal," *Optics letters* **2 6**, 148 (1978).

[5] Goldstein, D. H., "Mueller matrix dual-rotating retarder polarimeter.," *Applied optics* **31 31**, 6676–6683 (1992).

[6] Tuchin, V. V., "Polarized light interaction with tissues," *Journal of Biomedical Optics* **21**, 071114 (2016).

[7] Chang, J., He, H., Wang, Y., Huang, Y., Li, X., He, C., Liao, R., Zeng, N., Liu, S., and Ma, H., "Division of focal plane polarimeter-based 3x4 Mueller matrix microscope: a potential tool for quick diagnosis of human carcinoma tissues," *Journal of Biomedical Optics* **21**, 056002 (2016).

[8] Huang, T., Meng, R., Qi, J., Liu, Y., Wang, X., Chen, Y., Liao, R., and Ma, H., "Fast Mueller matrix microscope based on dual dofp polarimeters.," *Optics letters* **46 7**, 1676–1679 (2021).

[9] Suárez-Bermejo, J. C., de Sande, J. C. G., Santarsiero, M., and Piquero, G., "Mueller matrix polarimetry using full poincaré beams," *Optics and Lasers in Engineering* **122**, 134–141 (2019).

[10] Dubreuil, M., Rivet, S., Jeune, B. L., and Cariou, J. M., "Snapshot Mueller matrix polarimeter by wavelength polarization coding.," *Optics express* **15 21**, 13660–13668 (2007).

[11] Hagen, N., Oka, K., and Dereniak, E. L., "Snapshot Mueller matrix spectropolarimeter," *Optics Letters* **32**, 2100–2102 (2007).

[12] Lu, S. Y. and Chipman, R. A., "Interpretation of Mueller matrices based on polar decomposition," *Journal of The Optical Society of America A-optics Image Science and Vision* **13**, 1106–1113 (1996).

[13] Isola, P., Zhu, J.-Y., Zhou, T., and Efros, A. A., "Image-to-image translation with conditional adversarial networks," *2017 IEEE Conference on Computer Vision and Pattern Recognition (CVPR)* , 5967–5976 (2017).

[14] Wang, Z., Bovik, A. C., Sheikh, H. R., and Simoncelli, E. P., "Image quality assessment: from error visibility to structural similarity," *IEEE Transactions on Image Processing* **13**, 600–612 (2004).

[15] Ronneberger, O., Fischer, P., and Brox, T., "U-net: Convolutional networks for biomedical image segmentation," in [*MICCAI*], (2015).

[16] Li, C. and Wand, M., "Precomputed real-time texture synthesis with markovian generative adversarial networks," *European conference on computer vision. Springer* , 702–716 (2016).

[17] Si, L., Li, N., Huang, T., Du, S., Dong, Y., Yao, Y., and Ma, H., "Computational image translation from Mueller matrix polarimetry to bright-field microscopy," *Journal of Biophotonics* , e202100242 (2021).

[18] Wang, C., Qin, P., Lv, D., Wan, J., Sun, S., and Ma, H., "Characterization of anisotropy of the porous anodic alumina by the Mueller matrix imaging method," *Optics express* **28**(5), 6740–6754 (2020).